

Systematic Physics Constrained Parameter Estimation of Stochastic Differential Equations

Daniel Peavoy^{a,1}, Christian L. E. Franzke^{b,*}, Gareth O. Roberts^c

^a*Complexity Science Centre, University of Warwick, Coventry, UK*

^b*Meteorologisches Institut, KlimaCampus, Universität Hamburg, Hamburg, Germany*

^c*Department of Statistics, University of Warwick, Coventry, UK*

Abstract

We develop a systematic Bayesian framework for physics constrained parameter inference of stochastic differential equations (SDE) from partial observations. The physical constraints are derived for stochastic climate models but are applicable for many fluid systems. We first derive a condition for the Lyapunov stability of stochastic climate models based on energy conservation. Stochastic climate models are globally stable when a quadratic form, which is related to the cubic nonlinear operator, is negative definite. We develop a new algorithm for the efficient sampling of negative definite matrices and also for imputing unobserved data which improve the accuracy of the parameter estimates. Our algorithm can efficiently be implemented on GPU architectures leading to significant speed ups. We evaluate the performance of our framework on two conceptual climate models.

Keywords: Lyapunov Stability, Parameter Inference, Imputing Data, Stochastic Differential Equations, Physical Constraints, Stochastic Climate Models, GPU computing

2010 MSC: 86-08,

2010 MSC: 65C60,

2010 MSC: 86A10

1. Introduction

In many areas of science the inference of reduced order hybrid dynamic-stochastic models, which take the form of stochastic differential equations (SDE), from data is very important. For many applications running full resolution dynamical models is computationally prohibitive and in many situations one is mainly interested in large-scale features and not the exact evolution of the fast, small scale features, which typically determine the time step size. Thus, reduced order stochastic models are an attractive alternative. Examples are molecular dynamics, engineering turbulence, finance and climate science.

The inference of such models has been done using non-parametric methods (32, 14, 6) from partial observations. These non-parametric methods need very long time series for reliable parameter estimates and can be used only for very low-dimensional models because of the curse

*Meteorologisches Institut, KlimaCampus, Universität Hamburg, Grindelberg 5, 20144 Hamburg, Germany, christian.franzke@gmail.com

¹Present affiliation: Manufacturing Technology Centre, Coventry, UK

of dimension. More importantly, they do not necessarily obey conservation laws or stability properties of the full dimensional dynamical system. In many areas of science one can derive reduced order models from first principles (21, 24) such that certain fundamental properties of the full dynamics are still valid. These methods provide us with parametric forms for the model fitting. Physical constraints then not only constrain the parameters one has to estimate but they can also ensure global stability. Thus, there is a need for systematic physics constrained model and parameter estimation procedures (25, 22).

For instance, the climate system is governed by conservation laws like energy conservation. Based on this energy conservation property the normal form of stochastic climate models has been derived by (21) using the stochastic mode reduction procedure (18, 19, 20, 12, 13). This procedure allows the systematic derivation of reduced order models from first principles. This normal form provides a parametric form for parameter estimation from partial observations which we will use in this study.

The fundamental form of climate models is given by

$$\frac{d\mathbf{z}}{dt} = F + L\mathbf{z} + B(\mathbf{z}, \mathbf{z}) \quad (1)$$

where $\mathbf{z} \in \mathbb{R}^N$ denotes the N -dimensional state vector, F the external forcing, L a linear and B a quadratic nonlinear operator. The nonlinear operator B is conserving energy $\mathbf{z} \cdot B(\mathbf{z}, \mathbf{z})$. For current climate models N is of the order of $10^6 - 10^8$; thus, running complex climate models is computationally expensive. But for many applications like extended-range (periods of more than 2 weeks), seasonal and decadal climate predictions one is only interested in the large-scale circulation of the climate system and not whether there will be a cyclone over the North Atlantic on a particular day next year. The large-scale circulation can successfully be predicted using reduced order models (30, 1, 12, 13, 16).

The stochastic mode reduction procedure (18, 19, 20) provides a systematic framework for deriving reduced order climate models with a closure which takes account of the impact of the unresolved modes on the resolved modes. In order to derive reduced order models one splits the state vector $\mathbf{z} = \begin{pmatrix} \mathbf{x} \\ \mathbf{y} \end{pmatrix}$ into resolved \mathbf{x} and unresolved \mathbf{y} modes. The stochastic mode reduction procedure now enables us to systematically derive a reduced order climate model which only depends on \mathbf{x}

$$d\mathbf{x} = (\tilde{F} + \tilde{L}\mathbf{x} + \tilde{B}(\mathbf{x}, \mathbf{x}) + M(\mathbf{x}, \mathbf{x}, \mathbf{x}))dt + a(\mathbf{x}, \sigma)dW \quad (2)$$

where M denotes a cubic nonlinear term, W is the Wiener process and σ the diffusion parameters.

In this study we will develop a systematic Bayesian framework for the efficient estimation of the model parameters using Markov Chain Monte Carlo (MCMC) methods from partial observations. We are dealing with partial observations because we now only have knowledge of the few resolved modes \mathbf{x} and are ignorant about the many unresolved modes \mathbf{y} . We will derive conditions which ensure the global stability of the model. These conditions take the form of a negative definite matrix.

In section 2 we introduce stochastic climate models and derive conditions for Lyapunov stability. In section 3 we develop a Bayesian framework for the systematic estimation of the model parameters using physical constraints. Here we develop an efficient way of sampling negative-definite matrices. In section 4 we demonstrate the accuracy of our framework on conceptual climate models. In section 5 we show how to implement our framework on GPUs and achieve significant computational speed up. We summarize our results in section 6.

2. Stochastic Climate Models and Lyapunov Stability

Here we study the following D dimensional reduced order stochastic climate model (which has the same structural form as Eq. (2)):

$$dx_i = \left(\alpha_i + \sum_{j=1}^D \beta_{i,j} x_j + \sum_{j=1}^D \sum_{k=1}^j \gamma_{i,j,k} x_j x_k + \sum_{j=1}^D \sum_{k=1}^j \sum_{l=1}^k \lambda_{i,j,k,l} x_j x_k x_l \right) dt \quad (3a)$$

$$+ \sum_{j=1}^D a_{i,j} dW_j + \sum_{j=1}^D \sum_{k=1}^j b_{i,j,k} x_j dW_k. \quad (3b)$$

which we write for convenience in a more compact form

$$d\mathbf{x} = \mu(\mathbf{x}, \theta) dt + \sigma(\mathbf{x}, \theta) dW \quad (4)$$

The parameters α, β, γ and λ are written as one matrix $A \in \mathbb{R}^{D \times P}$. We allow for the inclusion of all possible linear, quadratic and cubic terms with forcing terms entering first, followed by linear, quadratic and the cubic terms. We include them into a matrix A as $A_{i,1} = \alpha_i$, $A_{i,j+1} = \beta_{i,j}$, $A_{i,j(j-1)/2+k+D+1} = \gamma_{i,j,k}$ and $A_{i,f(j,k,l)} = \lambda_{i,j,k,l}$. The index function for the cubic term is given by

$$f(j, k, l) = 1 + D + \frac{D(D+1)}{2} + \frac{j(j-1)(j+1)}{6} + \frac{k(k-1)}{2} + l. \quad (5)$$

Lyapunov stability implies that the energy associated with the cubic terms act as a nonlinear damping. The energy equation can be written as

$$\frac{1}{2} \frac{dE}{dt} = \sum_{i=1}^D x_i \frac{dx_i}{dt} = \sum_{i=1}^D \sum_{j=1}^D \sum_{k=1}^j \sum_{l=1}^k A_{i,f(j,k,l)} x_i x_j x_k x_l \quad (6)$$

We consider now the vector v with $\frac{D(D+1)}{2}$ components of the form $v_{(i-1)i/2+j} = x_i x_j$ with $1 \leq j \leq i \leq D$. Now we find a negative definite matrix M such that (21)

$$v^T M v = \frac{1}{2} \frac{dE}{dt} \leq 0 \quad (7)$$

A solution is as follows: Let matrix $M \in \mathbb{R}^{(D+1)D/2 \times (D+1)D/2}$ be

$$M_{(i-1)i/2+j, (k-1)k/2+l} = \begin{cases} A_{i,f(i,j,l)}, & \text{if } k > j \text{ and } l \leq j \\ 0, & \text{if } k > j \text{ and } l > j \\ A_{i,f(i,j,l)} + A_{i,f(i,j,k)}, & \text{if } k \leq j \text{ and } l < k \\ A_{i,f(i,j,l)}, & \text{if } k \leq j \text{ and } l = k \end{cases} \quad (8)$$

where $1 \leq j \leq i \leq D$ and $1 \leq l \leq k \leq D$.

In summary, the stochastic climate model in Eq. (4) is globally stable if the tensor M is negative definite and M determines the components of the cubic operator λ . This is an important result for the constrained parameter estimation of stochastic climate models (21, 25).

3. Physics Constraint Parameter Sampling

We use a Markov Chain Monte Carlo algorithm for the parameter inference which was proposed by (5) and (15). This algorithm overcomes the dependency between the diffusion parameters and the missing data by changing variables to the underlying Brownian motion $\mathbf{W} \in \mathbb{R}^d$ and conditioning on this when performing the parameter update.

Assuming we have the SDE in Eq. (4) and $\sigma(\mathbf{X}_t, \theta) \in \mathbb{R}^{d \times d}$ is invertible in its first argument then

$$d\mathbf{W}_t = \sigma^{-1}(\mathbf{X}_t, \theta)(d\mathbf{X}_t - \mu(\mathbf{X}_t, \theta)dt) \quad (9)$$

is a d -dimensional Brownian motion. We define a process \mathbf{Z} , which conditions on the endpoint \mathbf{x}_T , by

$$d\mathbf{X}_t = \sigma(\mathbf{X}_t, \theta)d\mathbf{Z}_t + \frac{\mathbf{x}_T - \mathbf{X}_t}{T - t}dt, \quad \mathbf{X}_0 = \mathbf{x}_0, \quad (10)$$

where T is the next observation time.

Let $\mathbf{X}_t = \mathbf{g}(\mathbf{Z}_t, \sigma)$ denote the transformation of all the data. The Jacobian determinant is equal to the product

$$\left| \frac{\partial \mathbf{g}}{\partial \mathbf{Z}} \right| = \prod_{i=1}^{N-1} |\sigma(\mathbf{X}_i, \theta)|. \quad (11)$$

Now we can write down an algorithm that does not degenerate as m increases. It is based on the reparametrisation of the conditional density of the data

$$p(\mathbf{X}|\theta, \sigma) = p(\mathbf{g}(\mathbf{Z}, \sigma)|\theta, \sigma) \left| \frac{\partial \mathbf{g}}{\partial \mathbf{Z}} \right|. \quad (12)$$

The density on the right hand side can be written as a Radon-Nikodym derivative of the law of \mathbf{Z} with respect to Brownian motion and so the dominating measure is parameter free (7). This means that the Metropolis-Hastings (MH) acceptance probability will have non zero numerator and denominator.

We sample σ according to Algorithm 1. We use zero-based numbering and consider there to be N observations and therefore, $N - 1$ observation intervals indexed $0 \dots N - 2$. We assume that the inter-observation times Δ are all equal and that there are $m - 1$ imputed points per interval, giving a time interval of $\delta = \Delta/m$. We use the notation $\mathbf{X}_i = \mathbf{X}_{t_i}$ and $\mu_i = \mu(\mathbf{X}_{t_i}, \theta)$. The extension to variable inter-observation times is straight forward. For simplicity, we write the algorithm for perfect observation of the system so that $\mathbf{X}_{im}, i = 0, \dots, N - 1$ are fixed.

To update missing data between observations we use an independence sampler as in (29) using the proposal process

$$d\mathbf{X}^* = \xi(\mathbf{X}^*, \mathbf{X}_T)dt + \mathbf{a}(\mathbf{X}^*, \sigma)d\mathbf{W}^*, \quad (13)$$

where \mathbf{X}_T is the next observation. This process will have measure that is absolutely continuous with respect to the target process in Eq. (4) because of their common diffusion function.

To update all of the missing data we propose a block at a time from Eq. (13) and then accept this according to the MH ratio. If the inter-observation interval is large then the acceptance rate may become very low and so one may sub-sample smaller blocks.

Algorithm 1 Sample parameters entering the diffusion matrix.

Draw $\sigma^* \sim q(\sigma^*|\sigma)$
 Initialise $\alpha = \log(q(\sigma|\sigma^*)) - \log(q(\sigma^*|\sigma)) + \log(p(\sigma^*)) - \log(p(\sigma))$
for $i = 0$ to $N - 2$ **do**
 for $j = 0$ to $m - 2$ **do**
 $Z_{im+j+1} = Z_{im+j} + a^{-1}(X_{im+j}, \sigma)(X_{im+j+1} - X_{im+j} - \frac{X_{im+m} - X_{im+j}}{m-j})$
 $X_{im+j+1}^* = X_{im+j}^* + \frac{X_{im+m} - X_{im+j}^*}{m-j} + a(X_{im+j}^*, \sigma^*)(Z_{im+j+1} - Z_{im+j})$
 $\alpha = \alpha + \log(\phi(X_{im+j+1}^*; X_{im+j}^* + \mu_{im+j}^* \delta, \delta \Sigma_{im+j}^*)) + \log |a(X_{im+j}^*, \sigma^*)|$
 $\quad - \log(\phi(X_{im+j+1}; X_{im+j} + \mu_{im+j} \delta, \delta \Sigma_{im+j})) - \log |a(X_{im+j}, \sigma)|$
 end for
end for
 Set $\{\sigma, X\} = \{\sigma^*, X^*\}$ with probability $\min(1, \exp(\alpha))$ else retain $\{\sigma, X\}$

101 For some interval i we set $X_0^* = X_{im}$ and $X_m^* = X_{(i+1)m}$ then we propose $X_1^* : X_{m-1}^*$ and accept
 102 or reject using the MH acceptance probability

$$\alpha = \frac{p_\delta(X_m^*|X_{m-1}^*, \theta) \prod_{j=0}^{m-2} p_\delta(X_{j+1}^*|X_j^*, \theta) q_\delta(X_{im+j+1}|X_{im+j}, \xi, \sigma)}{p_\delta(X_{(i+1)m}|X_{im+m-1}, \theta) \prod_{j=0}^{m-2} p_\delta(X_{im+j+1}|X_{im+j}, \theta) q_\delta(X_{j+1}^*|X_j^*, \xi, \sigma)}, \quad (14)$$

103 where p_δ is the transition density of the target

$$dX_t = \mu(X_t, \theta)dt + a(X_t, \theta)dW_t, \quad X_0 = x_0, \quad t \in [0, T] \quad (15)$$

104 over time interval δ and q_δ is the transition density of the proposal. We choose proposal processes
 105 so that given X_j^* , X_{j+1}^* is approximately Gaussian distributed. Eq. (13) is not a true Gaussian
 106 process because of the state dependent noise term. Details for updating the missing data are
 107 given in Algorithm 2.

108 Algorithms 1 and 2 are combined with standard MH updates for the parameters θ entering
 109 into the drift function. One could use Random-Walk proposals but in our case of polynomial
 110 models it is more efficient to implement another Gibbs sampling step. Repeatedly alternating be-
 111 tween these three steps will produce MCMC samples that can be used to estimate the parameters.
 112 In practice we increase the amount of missing data m until we see convergence in the marginal
 113 distributions of the parameters.

114 3.1. Sampling of Diffusion Paths

115 Now we discuss how we simulate diffusion paths from Eq. (3) that are conditioned upon start
 116 $X_0 = x_0$ and end $X_m = x_m$ points. The target density, with respect to Lebesgue measure, is the
 117 product

$$\pi(X_1 \cdots X_{m-1} | X_0 = x_0, X_m = x_m; \theta) = \prod_{i=0}^{m-1} p(\tau_{k+1}, x_{k+1} | \tau_k, x_k; \theta), \quad (16)$$

118 where now p is the transition density for the process in Eq. (3) and is, in practice, approximated
 119 by the Euler transition density. We consider the total time interval $\tau_m - \tau_0 = \Delta$ divided into m
 120 equidistant sub-intervals so that $\tau_{k+1} - \tau_k = \Delta/m = \delta$.

Algorithm 2 Sample missing data between observations.

```

for  $i = 0$  to  $N - 2$  do
  Set  $X_0^* = X_{im}$ 
  Set  $\alpha = 0$ 
  for  $j = 0$  to  $m - 2$  do
     $X_{j+1}^* \sim q_\delta(X_{j+1}^* | \xi(X_j^*, X_{im+m}), \sigma)$ 

     $\alpha = \alpha + \log(\phi(X_{j+1}^*; X_j^* + \delta\mu_j^*, \delta\Sigma_j^*) + \log(q_\delta(X_{im+j+1} | \xi(X_{im+j}, X_{im+m}), \sigma))$ 
     $- \log(\phi(X_{im+j+1}; X_{im+j} + \delta\mu_{im+j}, \delta\Sigma_{im+j})) - \log(q_\delta(X_{j+1}^* | X_j^*, \xi(X_j^*, X_{im+m}), \sigma))$ 

  end for
   $\alpha = \alpha + \log(\phi(X_{im+m}; X_{m-1}^* + \delta\mu_{m-1}^*, \delta\Sigma_{m-1}^*))$ 
   $- \log(\phi(X_{im+m}; X_{im+m-1} + \delta\mu_{im+m-1}, \delta\Sigma_{im+m-1}))$ 
  if  $\exp(\alpha) > \mathcal{U}(0, 1)$  then
    for  $j = 0$  to  $m - 2$  do
       $X_{im+j+1} = X_{j+1}^*$ 
    end for
  end if
end for

```

121 Having N observations, for each of $i = 0, 1, 2, \dots, N - 1$, X_{im} is an observation. Between every
 122 pair of observations the diffusion bridge will need to be simulated.

123 We use an independence sampler with proposal density of the form $q(X^* | X) = q(X^*)$. Here,
 124 we consider proposal processes of the form

$$dX^* = \xi(X_t^*, X_T)dt + a(X^*, \sigma)dW^*, \quad (17)$$

125 where $a(X^*, \sigma)$ is the same diffusion function as that in Eq. (4).

126 We use a Modified Linear Bridge proposal for sampling of parameters of the drift in Eq. (17).
 127 First we construct bridge distributions for general multivariate linear diffusions (4). If at time s
 128 we have $X_s = a$ and at time T , $X_T = b$ then the distribution of X_t for $0 \leq s < t \leq T$ can be
 129 shown to be Gaussian with mean

$$\nu_{a,b}(s, t) = \Gamma(t, T)\Gamma(s, T)^{-1}m_a^+(s, t) + \Gamma(s, T)^T(\Gamma(s, T)^T)^{-1}m_b^-(t, T) \quad (18)$$

130 where

$$\Gamma(s, t) = \int_s^t e^{(s-u)Q} \Sigma \Sigma^T e^{(t-u)Q^T} du,$$

$$m_x^+(s, t) = x + \int_s^t e^{(s-u)Q} r(u) du \quad \text{and} \quad m_x^-(s, t) = x - \int_s^t e^{(t-u)Q} r(u) du.$$

132 The covariance matrix is given by

$$\Sigma(s, t) = \Gamma(t, T)\Gamma(s, T)^{-1}\Gamma(s, t). \quad (19)$$

133 In general this matrix can be computed as follows: if we diagonalize Q so that $Q = U\Lambda U^{-1}$
 134 then compute the matrix A with components

$$A_{ij} = \frac{(U^{-1}\Sigma\Sigma^T U^{-T})_{ij}}{\Lambda_{ii} + \Lambda_{jj}} (e^{(t-s)\Lambda_{jj}} - e^{(s-t)\Lambda_{ii}}) \quad (20)$$

135 then

$$\Gamma(s, t) = \mathbf{U} \mathbf{A} \mathbf{U}^T. \quad (21)$$

136 In contrast to a linear bridge sampler here we update at each imputed point. This means
137 recomputing the matrices $\Gamma(s, t)$ at each point although \mathbf{Q} and \mathbf{U} are only calculated once.

138 3.2. Inference for Drift Parameters

139 Now we give details of the computational implementation of the sampling of parameters in
140 the drift function. Since the drift parameters enter linearly we can construct a Gibbs sampler
141 where their conditional posterior is Gaussian. This greatly improves the mixing of the Markov
142 Chain.

143 3.2.1. Gibbs Sampler

144 Consider N observations with time interval δ . We set $Y_t = X_{t+1} - X_t$ and let $\mathbf{U} \in \mathbb{R}^{N \times P}$ be
145 the design matrix of the data, scaled by δ . The columns of \mathbf{U} are indexed in the same way as the
146 columns of parameter matrix \mathbf{A} .

147 The log likelihood can be written

$$L(\mathbf{A}; \mathbf{X}) = -\frac{1}{2} \sum_{t=1}^{N-1} |\Sigma_t| - \frac{1}{2} \sum_{t=1}^{N-1} \sum_{i,j=1}^D \left(Y_{ti} - \sum_{k=1}^P U_{tk} A_{ik} \right) \Sigma_{tij}^{-1} \left(Y_{tj} - \sum_{k=1}^P U_{tk} A_{jk} \right) \quad (22)$$

148 where the instantaneous covariance matrix Σ_t is computed from $\Sigma_{t,jk}^{1/2} = (a_{j,k} + \sum_{l=1}^D b_{l,j,k} X_{t,l}) \Delta^{1/2}$.

149 We have DP parameters to infer in the matrix \mathbf{A} . We use a zero mean Gaussian prior with
150 covariance matrix $\Gamma \in \mathbb{R}^{DP \times DP}$. Let $\Lambda \in \mathbb{R}^{DP \times DP}$ be a matrix with components

$$\Lambda_{(i-1)P+j, (k-1)P+l} = \sum_{t=1}^{N-1} U_{tj} \Sigma_{tik}^{-1} U_{tl} + \Gamma_{(i-1)P+j, (k-1)P+l}^{-1} \quad (23)$$

151 where $i, k = 1 \dots D$ and $j, l = 1 \dots P$. Let $\mathbf{b} \in \mathbb{R}^{DP}$ with components

$$b_{(i-1)P+j} = \sum_{t,k} U_{t,j} \Sigma_{tik}^{-1} Y_{tk}. \quad (24)$$

152 The posterior mean $\mu_{(i-1)P+j}$ of $A_{i,j}$ is given by the solution of $\Lambda \boldsymbol{\mu} = \mathbf{b}$ and the posterior covari-
153 ance is $\text{Cov}(A_{i,j}, A_{k,l}) = \Lambda_{(i-1)P+j, (k-1)P+l}^{-1}$.

154 We applied the above Gibbs sampler to a large data set from a two dimensional model of the
155 form of Eq. (3) with random values for the diffusion parameters. We chose a fine observation
156 interval of $\delta = 10^{-3}$ and long observation period $T = 10,000$. Fig. 1 displays the trace plots for
157 all 20 parameters (note that the indices are from 0 rather than 1 as in the text). Using this large
158 data set the algorithm is able to reproduce the true values shown in red.

159 We performed a further simulation study to test the dependence of the posterior estimates
160 upon the data set used. We inferred all of the drift parameters for a simple two dimensional model
161 of the form of Eq. (3) using data sets of length $T = \{10, 100, 1000\}$ and with observation interval
162 $\Delta = \{0.1, 0.01, 0.001\}$. Note that the diffusion function is arbitrary in this model. The results
163 are shown in Table 1. For each parameter we estimated the posterior mean and the posterior
164 10th-90th percentiles. A cell is colored blue where the true value falls within this range. Note
165 that if we were using the true likelihood, rather than an approximation, then we would expect

there to be around 80% blue boxes. The error of the estimates for each data set can be quantified using the quadratic **Posterior Expected Loss** (PEL) function

$$f(\hat{\pi}, \mathbf{X}_{\text{obs}}) = \int_{\Theta} (\theta^* - \theta)^2 \hat{\pi}(\theta | \mathbf{X}_{\text{obs}}) d\theta, \quad (25)$$

where θ represents all of the parameters, $\hat{\pi}$ is the estimated posterior distribution and θ^* is the true value of the parameter.

We performed a test with both the Gibbs sampler and data imputation. In Tab. 2 the data is observed at interval $\Delta = 0.1$. The smaller intervals $\Delta = \{0.01, 0.001\}$ are obtained by imputing data with $m = \{10, 100\}$ respectively. The table shows that imputing data approximately doubles the Posterior Expected Loss. As expected the confidence intervals are broader but with more imputed data the algorithm can recover the true values. This shows that our data imputing strategy successfully improves the parameter estimates.

Our aim is to infer models that can be used for prediction. This can be problematic when dealing with non-linear models as some (generally unknown) regions of the parameter space will give solutions that explode to infinity with probability 1. This is a particular problem when, as exemplified by Table 1, large amounts of data are needed to regain the true values.

To demonstrate this problem we performed an inference on a two dimensional cubic model using $N = 1,000$ observations at $\Delta = 0.1$. For each inferred parameter value we then simulated the solution for $T = 100$. After this time we recorded whether the solution retained finite values or had exploded. The marginal posterior distributions of the cubic parameters are plotted in Fig. 2. Each plot shows two histograms: one in blue records the distribution of stable parameter values and in red are those that exploded. Notice that, when looking at the marginal distributions, the stable and unstable regions largely overlap; it is difficult to separate the two regions. In this case 40% of values were unstable. Tests (not shown) indicate that this is an even bigger problem in higher dimensions. Therefore, it is essential to use constraints on the parameter space to enable only physically meaningful solutions. The necessary conditions have been derived in section 2.

Thus, as shown above, when updating the drift parameters we ensure that \mathbf{M} is negative definite. In practice it is sufficient to check only whether the symmetric part $(\mathbf{M} + \mathbf{M}^T)/2$ is negative-definite. In the next section we will develop a systematic way of sampling negative definite matrices.

3.3. Sampling Negative Definite Matrices

To sample negative definite matrices we use the Component Wise algorithm (25). Here we sample the density of a $n \times n$ matrix \mathbf{M} , with normally distributed components, subject to the constraint that it is negative definite. This algorithm updates \mathbf{M} component wise and is based on the following property: an $n \times n$ matrix is negative definite if and only if all $k \leq n$ leading principal minors obey $|\mathbf{M}^{(k)}|(-1)^k > 0$. The k th principal minor is the determinant of the upper left $k \times k$ sub-matrix. Consider the parameters along the main diagonal. As they only enter \mathbf{M} once each will have an associated upper bound. The Algorithm 3 works by calculating the upper bound associated with the constraints from each principal minor. It does this to find the least upper bound and thereby the truncation point of the normal distribution.

Here, $\mathcal{N}_-(\mu, u, \sigma^2)$ is the right truncated normal distribution with mean μ , standard deviation σ and upper bound u . The off-diagonal parameters enter twice so there will be a quadratic function determining their limits for each leading principal minor. For parameters in element

Algorithm 3 Sample parameters along diagonal

```

for  $i = 1$  to  $n$  do
   $U_i = 0$ 
  for  $j = i$  to  $n$  do
     $x = -\left(\sum_{\substack{k \neq i \\ k=1}}^j (-1)^{i+k} M_{ik} |M_{\{-i\},\{-k\}}^{(j)}|\right) / |M_{\{-i\},\{-i\}}^{(j)}|$ 
  end for
  if  $x < U_i$  then
     $U_i = x$ 
  end if
   $M_{ii} \sim \mathcal{N}_-(\mu_i, U_i, \sigma_i^2)$ 
end for

```

207 $M_{ij}^{(k)}$ there will be an associated quadratic relation $a_{ij}^{(k)} M_{ij}^2 + b_{ij}^{(k)} M_{ij} + c_{ij}^{(k)} = 0$ where the coefficients
 208 are functions of the other parameters. These coefficients are found to be

$$a_{ij}^{(k)} = -|M_{/[i,j],/[i,j]}^{(k)}| \quad (26a)$$

$$b_{ij}^{(k)} = (-1)^{i+j} \sum_{\substack{k \neq i \\ k=1}}^{j-1} M_{jk} (-1)^{j-1+k} |M_{/[i,j],/[j,k]}^{(k)}| + (-1)^{i+j} \sum_{\substack{k \neq i \\ k=j+1}}^N M_{jk} (-1)^{j+k} |M_{/[i,j],/[j,k]}^{(k)}| \quad (26b)$$

$$+ (-1)^{i+j} \sum_{\substack{k \neq j \\ k=1}}^{i-1} M_{ik} (-1)^{i-1+k} |M_{/[i,j],/[i,k]}^{(k)}| + (-1)^{i+j} \sum_{\substack{k \neq j \\ k=i+1}}^N M_{ik} (-1)^{i+k} |M_{/[i,j],/[i,k]}^{(k)}| \quad (26c)$$

$$c_{ij}^{(k)} = \sum_{\substack{k \neq j \\ k=1}}^N M_{ik} (-1)^{i+k} \left(\sum_{\substack{l \neq i \\ l=1}}^{k-1} M_{jl} (-1)^{j-1+l} |M_{/[i,j],/[l,k]}^{(k)}| + \sum_{\substack{l \neq i \\ l=k+1}}^N M_{jl} (-1)^{j+l} |M_{/[i,j],/[l,k]}^{(k)}| \right) \quad (26d)$$

209 where $|M_{/[i,j],/[l,k]}^{(k)}|$ represents the k th principal minor with rows i and j and columns l and k
 210 removed. For each component M_{ij} this quadratic form can be solved to give upper and lower
 211 bounds on the parameter. The matrix M can be cycled through updating each parameter in turn.
 212 Algorithm 4 describes the sampling of off-diagonal elements using the coefficients in Eq. (26d).
 213 Here, the notation, $\mathcal{N}_-(\mu, u^-, u^+, \sigma^2)$ refers to the doubly truncated normal distribution with mean
 214 μ , left truncation u^- , right truncation u^+ and standard deviation σ .

215 To simulate from truncated normal distributions we are using the inverse Cumulative Density
 216 Function (CDF) method. One simply calculates the corresponding CDF of the lower and upper
 217 boundaries and then draws a uniform random variable between these numbers. Inverting the
 218 CDF gives a random variable from the Normal distribution restricted to this region.

219 For our problem we use the rejection sampler method proposed by (27). Rejection sampling
 220 from a distribution $h(x)$ is based on a proposal distribution $g(x)$ such that $h(x) \leq M g(x)$ holds for
 221 some constant M and all of the support of $h(x)$. For a one sided truncated Normal the exponential
 222 distribution is a good proposal. First it is translated to coincide with the truncation point then the
 223 rate parameter is optimized in order to closely match the tail of the Normal distribution.

$$g(z; \alpha, \mu^-) = \alpha \exp(-\alpha(z - \mu^-)) \mathbb{I}_{z \geq \mu^-} \quad (27)$$

Algorithm 4 Sample parameters off diagonal

```

for  $i = 1$  to  $n$  do
  for  $j = i + 1$  to  $n$  do
     $u^+ = \infty$ 
     $u^- = -\infty$ 
    for  $k = j$  to  $n$  do
      Calculate  $a_{ij}^{(k)}$ ,  $b_{ij}^{(k)}$  and  $c_{ij}^{(k)}$  and solve  $a_{ij}^{(k)}x^2 + b_{ij}^{(k)}x + c_{ij}^{(k)} = 0$ .
      Set  $mn = \min(x_1, x_2)$  and  $mx = \max(x_1, x_2)$ 
    end for
    if  $mx < u^+$  then
       $u^+ = mx$ 
    end if
    if  $mn > u^-$  then
       $u^- = mn$ 
    end if
     $M_{ij} \sim \mathcal{N}_-^+(\mu_{ij}, u^-, u^+, \sigma_{ij}^2)$ 
  end for
end for

```

224 The optimal value of α is calculated by maximizing the expected acceptance probability and is
 225 shown to be

$$\alpha^*(\mu^-) = \frac{\mu^- + \sqrt{(\mu^-)^2 + 4}}{2} \quad (28)$$

226 More details are given in (27).

227 We performed a numerical study to compare the standard Normal and Exponential proposals.
 228 The efficiency of proposing x from the standard normal then accepting if $x > \mu^-$ falls to
 229 approximately 0.023 while for the optimized exponential proposal is approximately 0.5.

230 For the doubly truncated Normal one uses either an exponential or uniform distribution, as a
 231 proposal, depending upon the size of the truncated region. If the following holds

$$u^+ > u^- + \frac{2\sqrt{e}}{u^- + \sqrt{(u^-)^2 + 4}} \exp\left(\frac{(u^-)^2 - u^- \sqrt{(u^-)^2 + 4}}{4}\right)$$

232 then it can be shown that the exponential is more efficient, otherwise the uniform is better (27).
 233 Fig. 3 shows both the uniform and exponential approximations for both cases.

234 We use Algorithms 3 and 4, along with the methods of sampling truncated Normal variables,
 235 to sample the stability matrix \mathbf{M} . We tested this algorithm on a three dimensional model with
 236 $T = 100$. In this case the dimension of \mathbf{M} is $n = D(D+1)/2 = 6$. Note that this MCMC algorithm
 237 still mixes well. Fig. 4 compares the posterior distributions estimated from the Component Wise
 238 Algorithm and the standard Gibbs sampler. Notice the large differences between the distributions
 239 in each case. Similar results (not shown) are obtained for the off diagonal parameters using
 240 Algorithm 4.

241 4. Results

242 4.1. Deterministic Double Well Potential Model

243 The first conceptual climate model we consider is a cubic model coupled to the chaotic
 244 Lorenz system (23). It is fully deterministic and consists of a slow variable representing a cli-
 245 mate process and three fast variables representing chaotic weather fluctuations. The slow variable
 246 moves inside a double well potential and is perturbed by the chaotic Lorenz system, which acts
 247 effectively as noise. The equations are as follows

$$\frac{dx}{dt} = x - x^3 + \frac{4}{90\epsilon}y_2 \quad (29a)$$

$$\frac{dy_1}{dt} = \frac{10}{\epsilon^2}(y_2 - y_1) \quad (29b)$$

$$\frac{dy_2}{dt} = \frac{1}{\epsilon^2}(28y_1 - y_2 - y_1y_3) \quad (29c)$$

$$\frac{dy_3}{dt} = \frac{1}{\epsilon^2}(y_1y_2 - \frac{8}{3}y_3). \quad (29d)$$

248 We now fit a one dimensional cubic SDE to the data. We just consider the general cubic form
 249 (21)

$$dX_t = (a_1 + a_2X_t + a_3X_t^2 + a_4X_t^3)dt + \sigma dW_t \quad (30)$$

250 and estimate all of the parameters $\{a_1, a_2, a_3, a_4, \sigma\}$ from sparse observations of the system: again
 251 using $\Delta = 10.0$ and $N = 1000$. To update the drift parameters we use the Gibbs sampler of
 252 Section 3.2.1. The estimated posterior distributions are shown in Fig. 6. A lot of imputed data is
 253 needed before the estimates start to converge towards the values predicted by homogenization but
 254 the inference demonstrates that there is enough information in the sparse data set if the likelihood
 255 is well approximated.

256 Figure 5 shows the predictive skill of the one dimensional reduced model for σ estimated
 257 for various m . Figures 5a and 5b show that the reduced model can reproduce the double well
 258 distribution of the full model although the separation of each well is underestimated for $m = 2$
 259 and $m = 4$ due to the larger noise. For $m \geq 8$ the model reproduces well the full models marginal
 260 distribution for x . It is not clear whether there is much difference between $m = 8$ and $m = 64$.
 261 However, observing Figures 5c and 5d we see that the autocorrelation function for the full model
 262 is much better approximated when $m = 64$. This shows that the ability of our framework to
 263 impute data is a powerful way of deriving accurate reduced order models.

264 4.2. Model Reduction for Triad Systems

265 Now we apply our model fitting procedure to a triad model with a high dimensional deter-
 266 ministic system with two slow, climate variables coupled to fast chaotic dynamics. The reduction
 267 strategy has two challenges: to successfully approximate the deterministic variables by a stochas-
 268 tic process and to be insensitive to a lack of time scale separation.

The full system is given by

$$\frac{dx_1}{dt} = \frac{b_1}{\epsilon} x_2 y_1 \quad (31a)$$

$$\frac{dx_2}{dt} = \frac{b_2}{\epsilon} x_1 y_1 \quad (31b)$$

$$\frac{dy_k}{dt} = \frac{b_3}{\epsilon} x_1 x_2 \delta_{1,k} - \operatorname{Re} \frac{ik}{2\epsilon^2} \sum_{p+q+k=0} \hat{u}_p^* \hat{u}_q^* \quad (31c)$$

$$\frac{dz_k}{dt} = -\operatorname{Im} \frac{ik}{2\epsilon^2} \sum_{p+q+k=0} \hat{u}_p^* \hat{u}_q^* . \quad (31d)$$

This system is stable provided that the energy is conserved $b_1 + b_2 + b_3 = 0$. We use the values $\mathbf{b} = \{0.9, -0.5 - 0.4\}$ and we choose a cut off of $\Lambda = 50$. We are interested in eliminating \mathbf{y} leaving equations for just x_1 and x_2 . The small parameter ϵ represents the time scales within the system. The variables \mathbf{y} have fastest time scale of order $O(1/\epsilon^2)$ compared to $O(1/\epsilon)$ for x_1 and x_2 . As $\epsilon \rightarrow 0$ we can use the method of homogenization for SDEs to eliminate the fast variables and this gives

$$dx_1(t) = \frac{b_1}{\gamma} (b_3 x_2^2(t) + \frac{\sigma^2}{2\gamma} b_2) x_1(t) dt + \frac{\sigma}{\gamma} b_1 x_2(t) dW_t \quad (32a)$$

$$dx_2(t) = \frac{b_2}{\gamma} (b_3 x_1^2(t) + \frac{\sigma^2}{2\gamma} b_1) x_2(t) dt + \frac{\sigma}{\gamma} b_2 x_1(t) dW_t, \quad (32b)$$

where unknown parameters σ and γ have been introduced. Here we estimate them using the Algorithms 1 and 2 from observations of the climate variables alone. For convenience we consider the inference problem where the model Eq. (32) is driven by two independent Brownian motions.

We apply the inference to a data set with total time $T = 500$ and observation interval $\Delta = 0.1$. We simulate the system for $\epsilon = \{0.01, 0.1, 0.25, 0.5, 0.8, 1.0\}$. Posterior estimates for the case $\epsilon = 0.8$ are shown in Fig. 7. This value corresponds to a moderately small, though realistic (12), amount of time scale separation. The vertical lines are the mean values of the posterior distributions for the case $\epsilon = 0.01$. Note that, as expected, there is a small discrepancy between the estimates for $\epsilon = 0.8$ and $\epsilon = 0.1$.

For the parameter estimation we assume the most general model (Eq. 3) and, thus, we have to estimate 28 unknown parameters. We estimated these using Algorithms 1 and 2, as well as the Gibbs sampling algorithm. We implemented the restricted parameter space using the constraints by using the element by element method. Fig. 8 shows the results for the drift parameters estimated for the case $\epsilon = 0.8$. As can be seen, for increasing the number of imputed data the posterior distributions tend to converge for most parameters.

We use the estimates from $m = 8$ to form a predictive model. Fig. 9 shows the autocorrelation function of mode x_1 of the full model with the one computed from the predictive model. As it can be seen, the decay of the autocorrelation function is very accurately captured. This is a particular hard test case because the time scale separation parameter $\epsilon = 0.8$ and we have only a very moderate, though realistic for the climate system (12), amount of time scale separation.

297 5. GPU Computing

298 In this section we describe the implementation of the basic algorithm for sampling parameters
 299 and missing data implemented on a Graphics Processing Unit (GPU) using NVIDIA's CUDA
 300 parallel programming environment. Recently statisticians have realized the potential for reduced
 301 computational time that can be achieved using massively parallel computation using GPUs. The
 302 GPU consists of a number of Streaming Multiprocesses (SM) each of which has a limited amount
 303 of fast on-chip shared memory. A SM is capable of performing and operation on 32 threads
 304 simultaneously whilst holding the remaining threads in memory. For the purpose of compatibility
 305 with different GPU configurations the CUDA programming model groups threads into thread
 306 blocks. Currently up to 1024 threads can be contained in a single thread block. Each block is
 307 sent to a SM and instructions on 32 threads executed simultaneously. The execution of these
 308 groups of threads hides the latency associated with memory request operations.

309 When converting a statistical algorithm for massively parallel computation one should con-
 310 sider how to decompose the problem into identical operations that can be performed with little
 311 dependence between them. Many data intensive applications in statistics are amenable to this sort
 312 of alteration. For example, (33) demonstrate the gains of using a GPU on a Bayesian mixture
 313 problem and report a speed up by a factor of 120 over the standard algorithm implemented on a
 314 single CPU. Using a different approach to dividing an algorithm for parallelisation is described
 315 by (17) and they report a speed up by a factor of about 280 over the CPU implementation.

316 Our inference procedure transfers naturally to a GPU implementation. The Markov nature of
 317 SDE data implies that the data set can be divided into independent blocks. In our implementation
 318 each thread is responsible for a single observation interval. The imputed data within that interval
 319 is sampled using the independence sampler proposal by a single thread.

320 The algorithm is split into two steps. Firstly the update of missing data and secondly the
 321 sampling of parameters. For perfect observations of the process, each thread in the first step
 322 can run without communication with threads responsible for neighboring data intervals. If there
 323 is observation error then the data at the observation time needs to be passed between threads
 324 causing a potential bottleneck in this step of the algorithm. We only consider the case of perfect
 325 observations.

326 The sampling of parameters is a global operation as it involves all of the data in the likelihood
 327 function. However, again due to the Markov property, each thread can compute the likelihood for
 328 a single data block. When this is done the threads need to synchronize before all the values can
 329 be added to form a single likelihood value. This is an example of a parallel reduction algorithm
 330 and is computed using a tree structure. Each evenly numbered thread receives a value from
 331 its neighboring thread and adds it to its own. Then every four threads sum their values and so
 332 on until there is just a single likelihood value. This is then added to the prior which can be
 333 computed by a single thread. The pseudo code for the update of missing data and parameters
 334 using the innovation scheme is shown below.

335 The algorithm can easily be generalized to multivariate problems. Each thread of the algo-
 336 rithm proposes new data \mathbf{Y} for a data block indexed by a parameter τ . As this part of the algorithm
 337 divides completely there is almost a linear increase in computational efficiency with number of
 338 threads for any given value of m . However, this is limited by the number of threads per block.
 339 The second stage, updating parameters, is slower as each thread requires access to some shared
 340 memory to read the updated parameters.

341 We tested our implementation on a GPU by applying it to a one dimensional Ornstein-

Algorithm 5 Parallel SDE inference with perfect observations. For each step Y has $m + 1$ components and is stored in local memory, unique to each thread. For the second step θ^* is stored in shared memory so is accessible to all threads.

```

 $\tau = \text{blockDim.x} \cdot \text{blockIdx.x} + \text{threadIdx.x}$ 
 $Y_0 = X_{\tau m}$ 
for  $i = 0$  to  $m - 2$  do
     $Y_{i+1} \sim P(Y_{i+1}|Y_i, X_{\tau m+m}, \theta)$  where  $P(\cdot|\cdot)$  is the modified linear bridge distribution.
     $\alpha = L(Y_{0:m}|\theta)/L(X_{\tau m:\tau m+m}|\theta)$ 
    accept  $Y$  with probability  $\alpha$ .
end for
 $\tau = 0$ 
 $\theta^* = \theta + \epsilon$ , where  $\epsilon \sim \mathcal{N}(0, \Sigma)$ 
 $\tau = \text{blockDim.x} \cdot \text{blockIdx.x} + \text{threadIdx.x}$ 
 $Y_0 = X_{\tau m}$ 
 $W_0 = 0, Y_0 = X_{\tau m}$ 
for  $i = 0$  to  $m - 2$  do
     $W_{i+1} = f^{-1}(Y_{i+1}, \theta)$  where  $f(\cdot)$  is one of the transformations for the innovation scheme.
     $Y_{i+1} = f(W_{i+1}, \theta^*)$ 
end for
 $\alpha_\tau = L(Y_{0:m}|\theta^*)/L(X_{\tau m:\tau m+m}|\theta) \times |J(f(X, \theta))|/|J(f(Y, \theta))|$  where  $J(\cdot)$  is the Jacobian for  $f(\cdot)$ .
SYNCTHREADS
for  $i = 1$  to  $\text{BlockDim.x} - 1$  do
    if  $(\tau = 0) \bmod 2i$  then
         $\alpha_\tau = \alpha_\tau + \alpha_{\tau+i}$ 
    end if
    SYNCTHREADS
end for
 $\tau = 0$ 
 $\alpha_0 = \alpha_0 + \pi(\theta^*)/\pi(\theta)$ , the prior distributions. Set  $\theta = \theta^*$  and  $X = Y$  with probability  $\alpha$ .

```

Uhlenbeck (OU) process model:

$$dx_t = \beta x_t dt + \sigma dW_t \quad (33)$$

where β is a coefficient and σ the scaling factor of the Wiener process dW_t . We compared the parameter estimates with those of the exact posterior distributions. The results, shown in Fig. 10, reveal that the estimated posteriors converge to the true distributions for increasing m .

Fig. 11 compares the real computational time of the GPU with the CPU implementations. Each plot shows how the running time increases with the amount of imputed data m . Notice that for small amounts of data, $N < 65$, the CPU implementation is faster. This is because the small number of threads does not compensate for the increased overheads and reduced clock speed of the GPU implementation. The potential of the parallel algorithm is demonstrated for values $N > 65$. Here, although both algorithms are linear in m , the GPU implementation is much faster. This is particularly true for large m with speed increases of factor 5 or more. On this particular GPU (in a standard laptop) the speed increase is not realized for $N > 257$. This is because as mentioned previously the algorithm will have to use multiple thread blocks so the threads would not have access to the same shared memory. As scientific computing expands its use of GPUs the number of threads per block should rise and the amount of shared memory increase.

6. Summary

Here we developed a systematic Bayesian framework for the inference of the parameter of SDEs constrained by the physics of the underlying system. The physical constraints not only constrain the parameter space but also enforce global stability of the reduced order models.

For conceptual climate models we use a constraint based on energy conservation which ensures Lyapunov stability of the effective SDE. This constraint takes the form of a negative definite matrix. We then develop a new algorithm for the sampling of negative definite matrices. We also develop a new algorithm for imputing data and show that imputing data improves the accuracy considerably of the parameter estimation. We demonstrated its power successfully on two conceptual climate models. Our algorithm can also be implemented on GPU computing systems with significant speed ups in computing time which shows its potential use for larger scale problems.

While we focused on climate models in this study our method is general enough that it can also be applied to other areas of fluid dynamics. Furthermore, also many other physical systems observe conservation laws and, thus, stability conditions can be derived which will be useful for parameter estimation procedures.

Acknowledgments This study received funding from the Natural Environment Research Council, the Engineering and Physical Sciences Research Council and the Deutsche Forschungsgemeinschaft.

References

- [1] Achatz, U. and G. Branstator, A two-layer model with empirical linear corrections and reduced order for studies of internal climate variability. *J. Atmos. Sci.*, 56, (1999) 3140-3160.
- [2] Ait-Sahalia, Y., Maximum likelihood estimation of discretely sampled diffusions: A closed-form approximation approach. *Econometrica*, 70, (2002) 223-262.
- [3] Ait-Sahalia, Y., Closed-form likelihood expansions for multivariate diffusions. *Annals Stat.*, 36, (2008) 906-937.
- [4] Barczykern, M. and P. Kern, Representations of multidimensional linear process bridges. *Rand. Oper. Stoch. Eq.*, 21, 159-189, (2013).
- [5] Chib, S., Pitt, M. and Shephard, N., Likelihood based inference for diffusion driven state space models. Working Paper, Nuffield College, Oxford University, (2004).

- [6] Crommelin, D. and E. Vanden-Eijnden, Reconstruction of diffusions using spectral data from timeseries. *Comm. Math. Sci.*, 4 (2006), 651-668.
- [7] Dargatz, C., Bayesian Inference for Diffusion Processes with Applications in Life Sciences. PhD thesis, Fakultät der Mathematik, Informatik und Statistik der Ludwig Maximilians Universität München, (2010).
- [8] Durham, G. B. and Gallant, A. R., Numerical techniques for maximum likelihood estimation of continuous-time diffusion processes. *J. Bus. Econ. Statist.*, 20 (2002), 297-316.
- [9] Eaton, M. L., Multivariate Statistics: A Vector Space Approach. Lecture Notes–Monograph. Series, Volume 53.
- [10] Eraker, B., MCMC analysis of diffusion models with application to finance. *J. Bus. Econ. Statist.*, 19 (2001), 177-191.
- [11] Elerian, O. S., Simulation estimation of continuous-time models with applications to finance. PhD thesis, Nuffield College, Oxford (1999).
- [12] Franzke, C., A. J. Majda and E. Vanden-Eijnden, Low-Order Stochastic Mode Reduction for a Realistic Barotropic Model Climate. *J. Atmos. Sci.*, 62 (2005), 1722-1745.
- [13] Franzke, C., and A. J. Majda, Low-Order Stochastic Mode Reduction for a Prototype Atmospheric GCM. *J. Atmos. Sci.*, 63 (2006), 457-479.
- [14] Friedrich, R., S. Siegert, J. Peinke, St. Lück, M. Siefert, M. Lindemann, J. Raethjen, G. Deuschl and G. Pfister, Extracting model equations from experimental data. *Phys. Lett. A*, 271 (2000), 217-222.
- [15] Golightly, A. and D. J. Wilkinson, Bayesian inference for nonlinear multivariate diffusion models observed with error. *Comp. Stat. Data Anal.*, 52 (2008), 1674-1693.
- [16] Kondrashov, D., S. Kravtsov and M. Ghil, Empirical mode reduction in a model of extratropical low-frequency variability. *J. Atmos. Sci.*, 63 (2006), 1859-1877.
- [17] Lee, A., Yau, Ch., Giles, M. B., Doucet, A. and Holmes, C. C., On the Utility of Graphics Cards to Perform Massively Parallel Simulation of Advanced Monte Carlo Methods. *J. Comp. Graph. Stat.*, 19 (2010), 769-789.
- [18] Majda, A. J., I. Timofeyev and E. Vanden-Eijnden, Models for stochastic climate prediction. *Proc. Nat. Acad. Sci. USA*, 96 (1999), 14687-14691.
- [19] Majda, A. J., I. Timofeyev and E. Vanden-Eijnden, A mathematical framework for stochastic climate models. *Commun. Pure Appl. Math.*, 54 (2001), 891-974.
- [20] Majda, A. J., C. Franzke and B. Khouider, An applied mathematics perspective on stochastic modelling for climate. *Phil. Trans. R. Soc. A*, 366 (2008), 2429-2455.
- [21] Majda, A. J., C. Franzke and D. Crommelin, Normal forms for reduced stochastic climate models. *Proc. Nat. Acad. Sci. USA*, 106, (2009) 3649-3653. doi: 10.1073/pnas.0900173106
- [22] Majda, A. J. and J. Harlim, Physics constrained nonlinear regression models for time series. *Nonlinearity*, 26, (2013) 201-217.
- [23] Mitchell, L. and Gottwald, G. A., Data Assimilation in Slow-Fast Systems Using Homogenized Climate Models. *J. Atmos. Sci.*, 69, (2012) 1359-1377.
- [24] Pavliotis, G. A. and A. M. Stuart, *Multiscale methods*, Springer Verlag, (2008) 310pp.
- [25] Peavoy, D., Methods of likelihood based inference for constructing stochastic climate models, PhD thesis, University of Warwick, (2013) 232pp.
- [26] Pedersen, A. R., A new approach to maximum likelihood estimation for stochastic differential equations based on discrete observations. *Scand. J. Statist.*, 22, (1995) 55-71.
- [27] Robert, C., Simulation of truncated normal variables. *Stat. Comp.*, 5, (1995) 121-125.
- [28] Roberts, G. O., A. Gelman and W. R. Gilks, Weak convergence and optimal scaling of random walk Metropolis algorithms. *Ann. App. Prob.*, 7, (1997) 110-120.
- [29] Roberts, G. O. and Stramer, O., On inference for partially observed nonlinear diffusion models using the Metropolis-Hastings algorithm. *Biometrika*, 88, (2001) 603-621.
- [30] Selten, F. M., An efficient description of the dynamics of barotropic flow. *J. Atmos. Sci.*, 52, (1995) 915-936.
- [31] Shephard, N. and Pitt, M. K., Likelihood analysis of non-Gaussian measurement time series. *Biometrika*, 84, (1997) 653-667.
- [32] Siegert, S., R. Friedrich and J. Peinke, Analysis of data sets of stochastic systems. *Phys. Lett. A*, 243 (1998), 275-280.
- [33] Suchard, M. A., Wang, Q., Chan, C., Frelinger, J., Cron, A. and West, M., Understanding GPU Programming for Statistical Computation: Studies in Massively Parallel Massive Mixtures. *J. Comp. Graph. Stat.*, 19 (2010), 419-438.

	$T = 10$			$T = 100$			$T = 1000$		
	0.1	0.01	0.001	0.1	0.01	0.001	0.1	0.01	0.001
$A_{00} = 0$	2.18 (-2.5,6.89)	-0.44 (-4.79,3.74)	-1.95 (-6.07,2.2)	-0.13 (-1.07,0.77)	0.65 (-0.29,1.6)	0.64 (-0.28,1.58)	0.02 (-0.13,0.17)	0.01 (-0.13,0.17)	0.02 (-0.13,0.18)
$A_{01} = 5$	-2.04 (-7.23,3.04)	4.86 (0.84,9.04)	6.21 (2.31,10.12)	2.54 (1.78,3.28)	4.73 (3.93,5.51)	5.22 (4.43,6.03)	2.84 (2.7,2.97)	4.59 (4.45,4.73)	4.86 (4.73,5)
$A_{02} = 0$	2.63 (-0.16,5.39)	2.15 (-0.17,4.49)	1.63 (-0.66,4)	0.45 (-0.52,1.41)	0.58 (-0.42,1.6)	0.13 (-0.89,1.13)	-0.08 (-0.22,0.05)	-0.14 (-0.27,0)	-0.19 (-0.32,-0.04)
$A_{03} = 0$	1.54 (-2.75,5.84)	-0.17 (-3.12,2.76)	0.26 (-2.62,3.2)	0.27 (-0.38,0.93)	0.01 (-0.72,0.73)	-0.17 (-0.88,0.54)	-0.01 (-0.08,0.06)	0 (-0.07,0.06)	0 (-0.07,0.06)
$A_{04} = 0$	-3.51 (-8.17,1.13)	0.61 (-3.4,3)	1.3 (-2.32,5.07)	-0.96 (-2.09,0.2)	-0.58 (-1.8,0.68)	-0.07 (-1.3,1.16)	-0.01 (-0.04,0.01)	-0.02 (-0.04,0.01)	-0.02 (-0.05,0.01)
$A_{05} = 0$	0.32 (-2.19,2.81)	0 (-2.31,2.31)	0.19 (-2.11,2.49)	0.66 (-0.11,1.43)	0.02 (-0.79,0.84)	-0.27 (-1.05,0.55)	0 (-0.06,0.07)	0.01 (-0.06,0.07)	0 (-0.07,0.07)
$A_{06} = -3$	-0.88 (-2.96,1.24)	-2.58 (-4.3,-0.87)	-3.17 (-4.83,-1.49)	-1.8 (-2,-1.6)	-2.92 (-3.12,-2.71)	-3.05 (-3.25,-2.85)	-1.71 (-1.77,-1.65)	-2.75 (-2.81,-2.69)	-2.91 (-2.97,-2.85)
$A_{07} = 0$	0.58 (-1.87,3.06)	-1.32 (-3.32,0.7)	-1.48 (-3.54,0.52)	0.05 (-0.49,0.58)	-0.07 (-0.66,0.51)	-0.22 (-0.79,0.37)	-0.02 (-0.07,0.04)	-0.01 (-0.06,0.05)	0 (-0.05,0.06)
$A_{08} = 0$	-0.83 (-3.1,3.1)	-0.28 (-2.31,1.76)	-0.18 (-2.21,1.86)	-0.48 (-1.03,0.07)	-0.37 (-0.96,0.23)	-0.16 (-0.75,0.42)	-0.02 (-0.08,0.03)	-0.01 (-0.06,0.04)	-0.01 (-0.07,0.04)
$A_{09} = 0$	0.71 (-0.11,1.53)	-0.4 (-1.16,0.38)	-0.49 (-1.26,0.27)	0.33 (-0.02,0.67)	0.04 (-0.3,0.39)	0.09 (-0.25,0.44)	0.08 (0.02,0.13)	0.1 (0.04,0.16)	0.12 (0.05,0.17)
$A_{10} = 0$	-0.38 (-5.19,4.24)	-2.21 (-6.44,2.03)	-1.17 (-5.21,2.9)	-0.31 (-1.22,0.61)	-0.18 (-1.1,0.75)	0.06 (-0.89,0.99)	0.02 (-0.13,0.17)	0.05 (-0.1,0.2)	0.05 (-0.1,0.2)
$A_{11} = 0$	-2.93 (-8.11,2.15)	2.42 (-1.64,6.48)	1.67 (-2.29,5.64)	0.88 (0.1,1.64)	0.39 (-0.4,1.19)	0.33 (-0.48,1.12)	-0.06 (-0.2,0.08)	0.11 (-0.03,0.25)	0.11 (-0.04,0.24)
$A_{12} = 5$	5.96 (3.22,8.68)	4.2 (1.89,6.63)	4.72 (2.33,7.09)	1.68 (0.72,2.65)	4.56 (3.52,5.57)	5.09 (4.08,6.12)	2.88 (2.74,3.02)	4.7 (4.56,4.84)	4.98 (4.84,5.11)
$A_{13} = 0$	2.68 (-1.67,6.93)	-1.41 (-4.36,1.57)	-1.88 (-4.74,1.02)	-1.05 (-1.72,-0.38)	-0.61 (-1.33,0.1)	-0.74 (-1.46,-0.02)	-0.01 (-0.08,0.05)	-0.03 (-0.1,0.03)	-0.03 (-0.09,0.04)
$A_{14} = 0$	-1.13 (-5.84,3.6)	4.67 (1.01,8.45)	4.23 (0.47,7.92)	1.39 (0.24,2.55)	0.78 (-0.44,2.03)	0.91 (-0.33,2.14)	0.02 (-0.01,0.05)	0.03 (0.0,0.05)	0.03 (0.0,0.05)
$A_{15} = 0$	0.42 (-2.07,2.94)	-0.6 (-2.88,1.77)	-0.84 (-3.13,1.45)	-0.22 (-1.01,0.56)	-0.11 (-0.9,0.7)	-0.24 (-1.06,0.55)	0 (-0.07,0.06)	-0.01 (-0.08,0.05)	-0.02 (-0.09,0.04)
$A_{16} = 0$	-0.82 (-2.94,1.29)	0.12 (-1.61,1.83)	0.39 (-1.26,2)	-0.08 (-0.28,0.12)	-0.04 (-0.24,0.17)	-0.02 (-0.22,0.19)	-0.03 (-0.09,0.03)	-0.08 (-0.14,-0.02)	-0.09 (-0.15,-0.03)
$A_{17} = 0$	-0.46 (-2.95,2.04)	-3.21 (-5.28,-1.22)	-2.97 (-4.99,-0.93)	-0.71 (-1.25,-0.17)	-0.66 (-1.24,-0.08)	-0.78 (-1.35,-0.19)	0.01 (-0.05,0.06)	-0.01 (-0.06,0.04)	0 (-0.05,0.05)
$A_{18} = 0$	0.66 (-1.5,2.86)	1.33 (-0.71,3.35)	1.63 (-0.41,3.6)	0.65 (0.11,1.22)	0.45 (-0.13,1.04)	0.58 (-0.01,1.18)	0.06 (0.01,0.12)	0.02 (-0.03,0.08)	0.03 (-0.02,0.09)
$A_{19} = -3$	-2.61 (-3.44,-1.78)	-3.23 (-4.02,-2.45)	-3.47 (-4.24,-2.69)	-1.46 (-1.8,-1.12)	-2.73 (-3.07,-2.38)	-3.04 (-3.39,-2.7)	-1.75 (-1.81,-1.69)	-2.81 (-2.87,-2.75)	-2.98 (-3.04,-2.92)
	8.48	5.25	4.96	1.19	0.37	0.36	0.43	0.02	0.01

Table 1: Drift parameter estimates for a two dimensional cubic model with arbitrary diffusion function. On the left is the true value of the parameter. The length of the data set used for the inference is labeled as T and the observation interval is $\Delta = \{0.1, 0.01, 0.001\}$. In each cell the parameter is estimated from the posterior mean and in brackets is shown the 10th-90th percentiles of the posterior. The blue coloring is where the true value falls in this range. The bottom of the table shows the Posterior Expected Loss in each case.

	$T = 10$			$T = 100$			$T = 1000$		
	0.1	0.01	0.001	0.1	0.01	0.001	0.1	0.01	0.001
$A_{00} = 0$	2.18 (-2.5,6.89)	-2.46 (-8.46,3.52)	-2.59 (-8.35,3.24)	-0.13 (-1.07,0.77)	-0.68 (-1.84,0.5)	-0.69 (-1.85,0.49)	0.02 (-0.13,0.17)	-0.08 (-0.27,0.09)	-0.08 (-0.26,0.09)
$A_{01} = 5$	-2.04 (-7.23,3.04)	4.99 (-0.7,10.61)	4.84 (-0.49,10.22)	2.54 (1.78,3.28)	4.89 (3.83,5.97)	4.76 (3.74,5.79)	2.84 (2.7,2.97)	5.04 (4.87,5.21)	4.88 (4.71,5.03)
$A_{02} = 0$	2.63 (-0.16,5.39)	0.61 (-2.94,4.05)	0.39 (-2.95,3.75)	0.45 (-0.52,1.41)	-0.06 (-1.42,1.3)	-0.2 (-1.49,1.13)	-0.08 (-0.22,0.05)	-0.26 (-0.44,-0.08)	-0.28 (-0.45,-0.09)
$A_{03} = 0$	1.54 (-2.75,5.84)	3.25 (-1.23,8.07)	3.26 (-1.07,7.77)	0.27 (-0.38,0.93)	0.67 (-0.34,1.67)	0.59 (-0.41,1.59)	-0.01 (-0.08,0.06)	0.02 (-0.06,0.1)	0.02 (-0.06,0.09)
$A_{04} = 0$	-3.51 (-8.17,1.13)	-2.53 (-7.76,2.61)	-2.53 (-7.61,2.41)	-0.96 (-2.09,0.2)	-1.6 (-3.35,0.18)	-1.41 (-3.14,0.27)	-0.01 (-0.04,0.01)	-0.03 (-0.05,0)	-0.02 (-0.05,0)
$A_{05} = 0$	0.32 (-2.19,2.81)	1.85 (-1.6,5.2)	1.85 (-1.43,5.11)	0.66 (-0.11,1.43)	1.18 (0.03,2.32)	1.12 (-0.02,2.25)	0 (-0.06,0.07)	0.05 (-0.04,0.13)	0.05 (-0.04,0.13)
$A_{06} = -3$	-0.88 (-2.96,1.24)	-4.06 (-6.63,-1.76)	-4.02 (-6.5,-1.79)	-1.8 (-2,-1.6)	-3.19 (-3.44,-2.94)	-3.06 (-3.3,-2.83)	-1.71 (-1.77,-1.65)	-3.01 (-3.08,-2.94)	-2.92 (-2.98,-2.85)
$A_{07} = 0$	0.58 (-1.87,3.06)	0.44 (-2.27,3.17)	0.53 (-2.05,3.23)	0.05 (-0.49,0.58)	0.43 (-0.37,1.27)	0.39 (-0.42,1.19)	-0.02 (-0.07,0.04)	0.03 (-0.04,0.09)	0.03 (-0.03,0.09)
$A_{08} = 0$	-0.83 (-3.1,3.1)	-2.22 (-4.98,0.62)	-2.12 (-4.84,0.65)	-0.48 (-1.03,0.07)	-1 (-1.86,-0.14)	-0.92 (-1.76,-0.09)	-0.02 (-0.08,0.03)	-0.02 (-0.09,0.05)	-0.02 (-0.09,0.05)
$A_{09} = 0$	0.71 (-0.11,1.53)	1.29 (0.06,2.61)	1.33 (0.1,2.6)	0.33 (-0.02,0.67)	0.7 (0.17,1.2)	0.71 (0.19,1.2)	0.08 (0.02,0.13)	0.14 (0.05,0.23)	0.15 (0.06,0.23)
$A_{10} = 0$	-0.38 (-5.19,4.24)	-4.63 (-10.46,0.84)	-4.46 (-10.07,0.86)	-0.31 (-1.22,0.61)	0.66 (-0.55,1.87)	0.6 (-0.51,1.75)	0.02 (-0.13,0.17)	-0.02 (-0.2,0.16)	-0.01 (-0.2,0.16)
$A_{11} = 0$	-2.93 (-8.11,2.15)	2.18 (-3.8,8.3)	2.24 (-3.53,8.27)	0.88 (0.1,1.64)	0.1 (-0.89,1.09)	0.15 (-0.82,1.14)	-0.06 (-0.2,0.08)	0.08 (-0.09,0.26)	0.11 (-0.06,0.29)
$A_{12} = 5$	5.96 (3.22,8.68)	8.28 (4.62,11.9)	7.82 (4.39,11.36)	1.68 (0.72,2.65)	5.8 (4.52,7.07)	5.57 (4.36,6.81)	2.88 (2.74,3.02)	5.05 (4.88,5.22)	4.89 (4.72,5.05)
$A_{13} = 0$	2.68 (-1.67,6.93)	4.03 (-0.84,9.1)	4.08 (-0.63,8.96)	-1.05 (-1.72,-0.38)	-0.83 (-1.76,0.11)	-0.81 (-1.72,0.1)	-0.01 (-0.08,0.05)	-0.01 (-0.09,0.08)	-0.01 (-0.09,0.08)
$A_{14} = 0$	-1.13 (-5.84,3.6)	0.2 (-5.79,6.51)	0.02 (-5.85,6.12)	1.39 (0.24,2.55)	0.12 (-1.44,1.66)	0.07 (-1.43,1.61)	0.02 (-0.01,0.05)	0.03 (0.0,0.06)	0.03 (0.0,0.06)
$A_{15} = 0$	0.42 (-2.07,2.94)	1.49 (-1.84,5)	1.59 (-1.64,4.85)	-0.22 (-1.01,0.56)	0.15 (-0.89,1.18)	0.2 (-0.8,1.19)	0 (-0.07,0.06)	0.01 (-0.07,0.08)	0 (-0.07,0.08)
$A_{16} = 0$	-0.82 (-2.94,1.29)	-3.07 (-5.88,-0.39)	-3.14 (-5.86,-0.5)	-0.08 (-0.28,0.12)	-0.15 (-0.45,0.15)	-0.15 (-0.45,0.15)	-0.03 (-0.09,0.03)	-0.07 (-0.15,0.02)	-0.08 (-0.17,0)
$A_{17} = 0$	-0.46 (-2.95,2.04)	-1.37 (-4.65,1.87)	-1.17 (-4.45,1.91)	-0.71 (-1.25,-0.17)	-0.59 (-1.36,0.19)	-0.57 (-1.31,0.17)	0.01 (-0.05,0.06)	0.05 (-0.02,0.12)	0.05 (-0.03,0.12)
$A_{18} = 0$	0.66 (-1.5,2.86)	0.3 (-2.65,3.15)	-0.01 (-2.73,2.67)	0.65 (0.11,1.22)	0.24 (-0.51,0.99)	0.18 (-0.54,0.92)	0.06 (0.01,0.12)	0.02 (-0.04,0.08)	0.02 (-0.04,0.08)
$A_{19} = -3$	-2.61 (-3.44,-1.78)	-4.44 (-5.58,-3.38)	-4.1 (-5.16,-3.13)	-1.46 (-1.8,-1.12)	-3.09 (-3.53,-2.66)	-2.94 (-3.36,-2.55)	-1.75 (-1.81,-1.69)	-3.06 (-3.14,-2.99)	-2.97 (-3.04,-2.9)
	8.48	11.06	10.32	1.19	0.76	0.68	0.43	0.01	0.01

Table 2: Drift parameter estimates for a two dimensional cubic model with arbitrary diffusion function. On the left is the true value of the parameter. The data used is the same as that of Table 1 sampled at the $\Delta = 0.1$ interval. In this case data is imputed to obtain the intervals $\Delta = \{0.01, 0.001\}$. The bottom of the table shows the Posterior Expected Loss in each case.

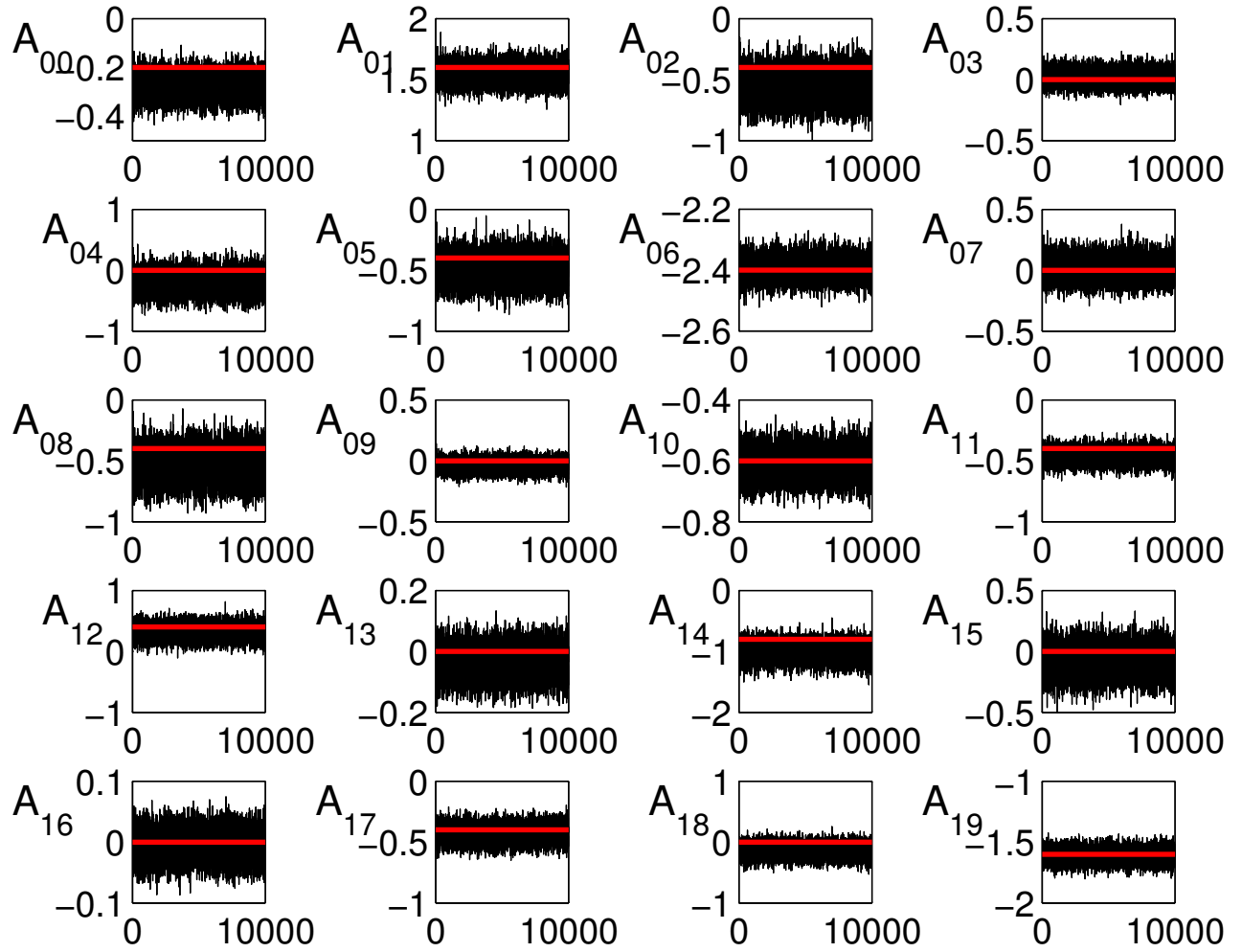


Figure 1: Output of a Gibbs sampler for 20 drift parameters of a two dimensional model from Eq. (3). The observation interval is $\delta = 10^{-3}$ and $T = 10,000$. The true values are shown in red.

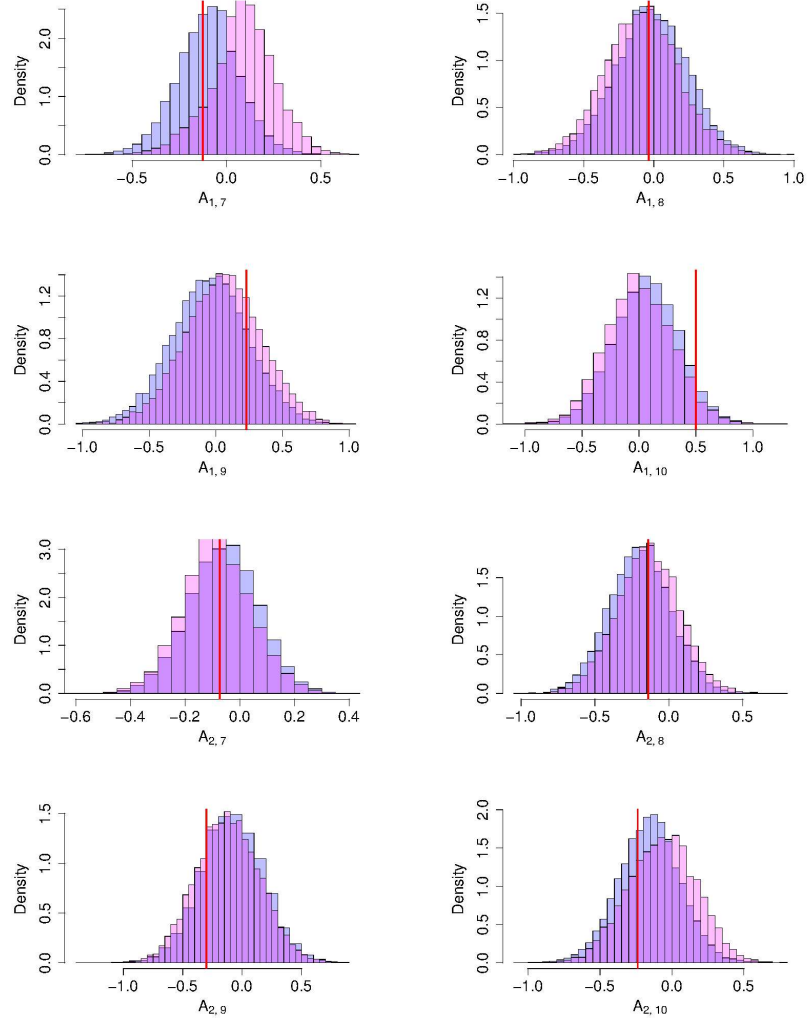


Figure 2: Marginal distributions of the cubic parameters inferred from a data set with $N = 1,000$ observations at interval $\Delta = 0.1$. The blue histogram shows the parameters that gave stable solutions to the SDE, while the red is for those that gave unstable solutions. The true values are given by the red lines.

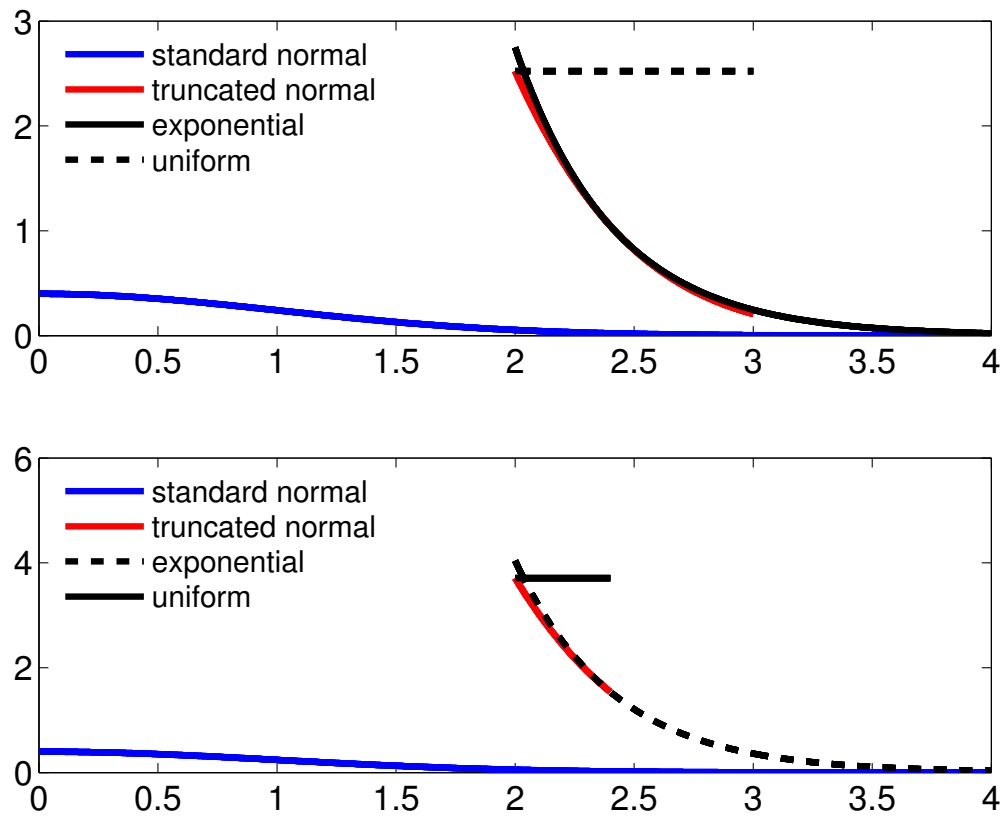


Figure 3: Doubly truncated normal distribution. The top figure has $u^- = 2$ and $u^+ = 3$ and is better approximated with the exponential distribution. The bottom figure has $u^- = 2$ and $u^+ = 2.5$ and the uniform is more efficient.

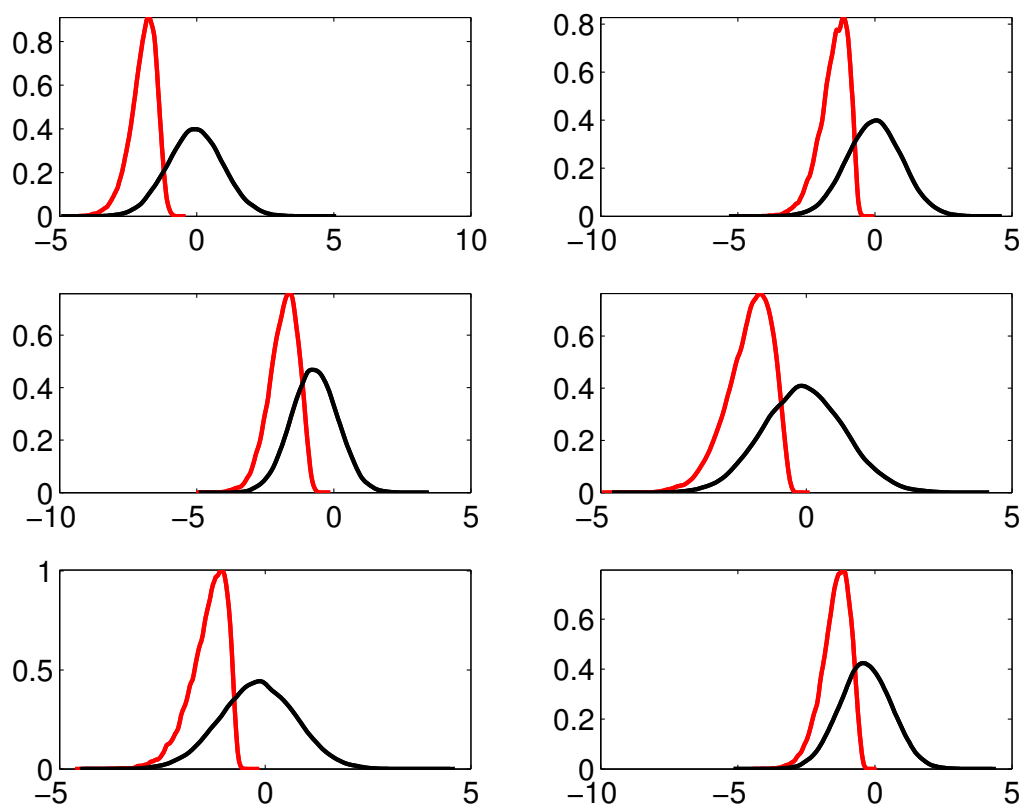
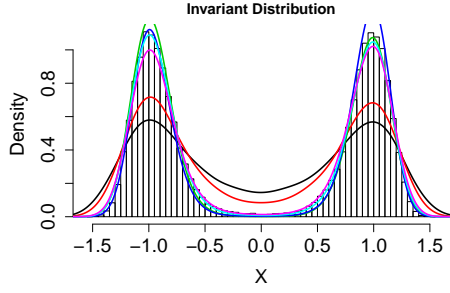
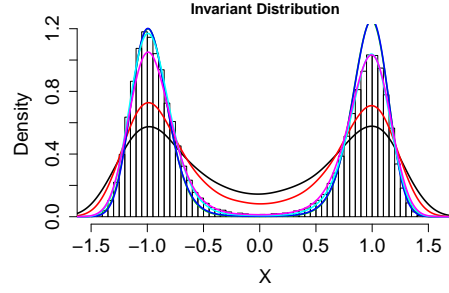


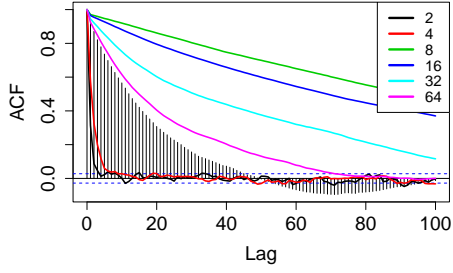
Figure 4: Output from Algorithm 1 (red) compared to sampling directly using the Gibbs sampler (black).



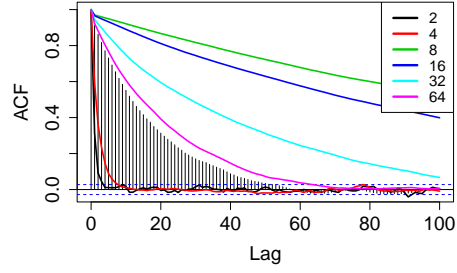
(a) Invariant distribution with $\epsilon = 0.1$. Histogram is for the full system, the lines correspond to different m .



(b) Invariant distribution with $\epsilon = 0.01$. Histogram is for the whole system, the lines correspond to different m .

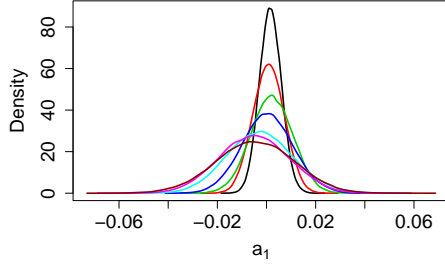


(c) Autocorrelation function for $\epsilon = 0.1$. Bars are for the full system.

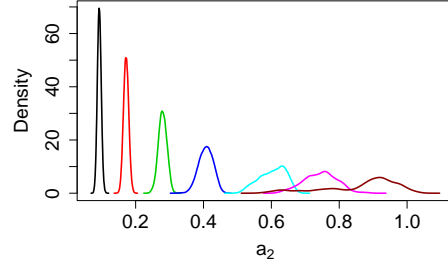


(d) Autocorrelation function for $\epsilon = 0.01$. Bars are for the full system.

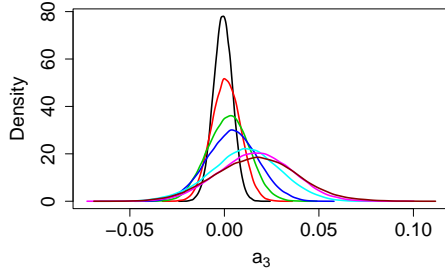
Figure 5: Predictive statistics for the reduced double well model coupled to chaotic Lorenz system: Eq. (29d) for two values of ϵ . In each plot the lines correspond to the inferred one dimensional model for different m .



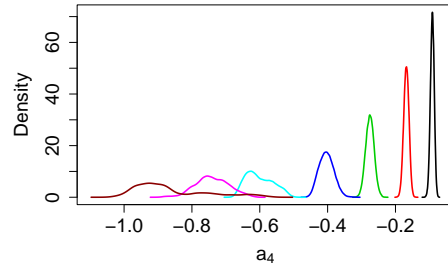
(a) Theoretical value 0



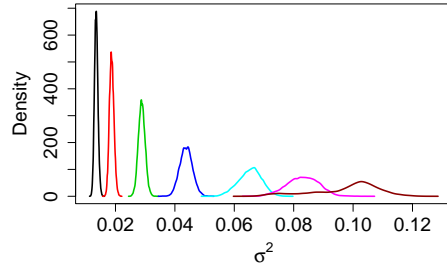
(b) Theoretical value 1



(c) Theoretical value 0



(d) Theoretical value -1



(e) Theoretical value 0.11

Figure 6: Posterior distribution estimates from MCMC output applied to a sparse data set ($\Delta = 10$). Different distributions correspond to increasing amounts of missing data. The distribution in brown, for $m = 64$, agrees with the theoretical values predicted by the homogenization procedure.

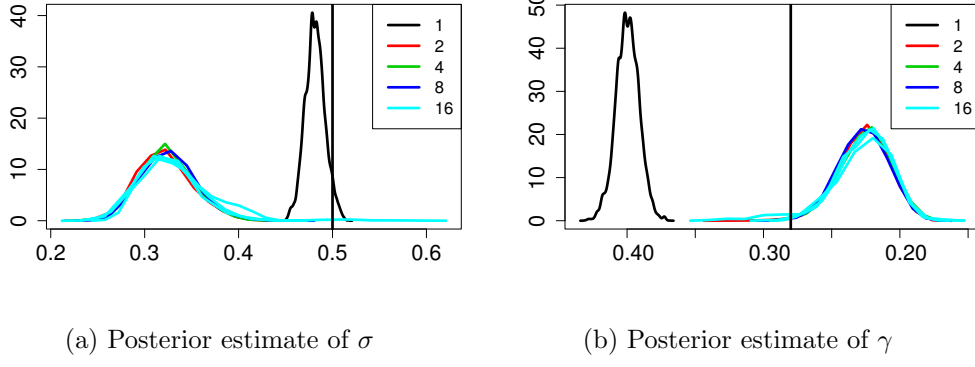


Figure 7: Posterior estimates of parameters in Eq. 32. This data set is simulated from Eq. (31) with $\epsilon = 0.8$.

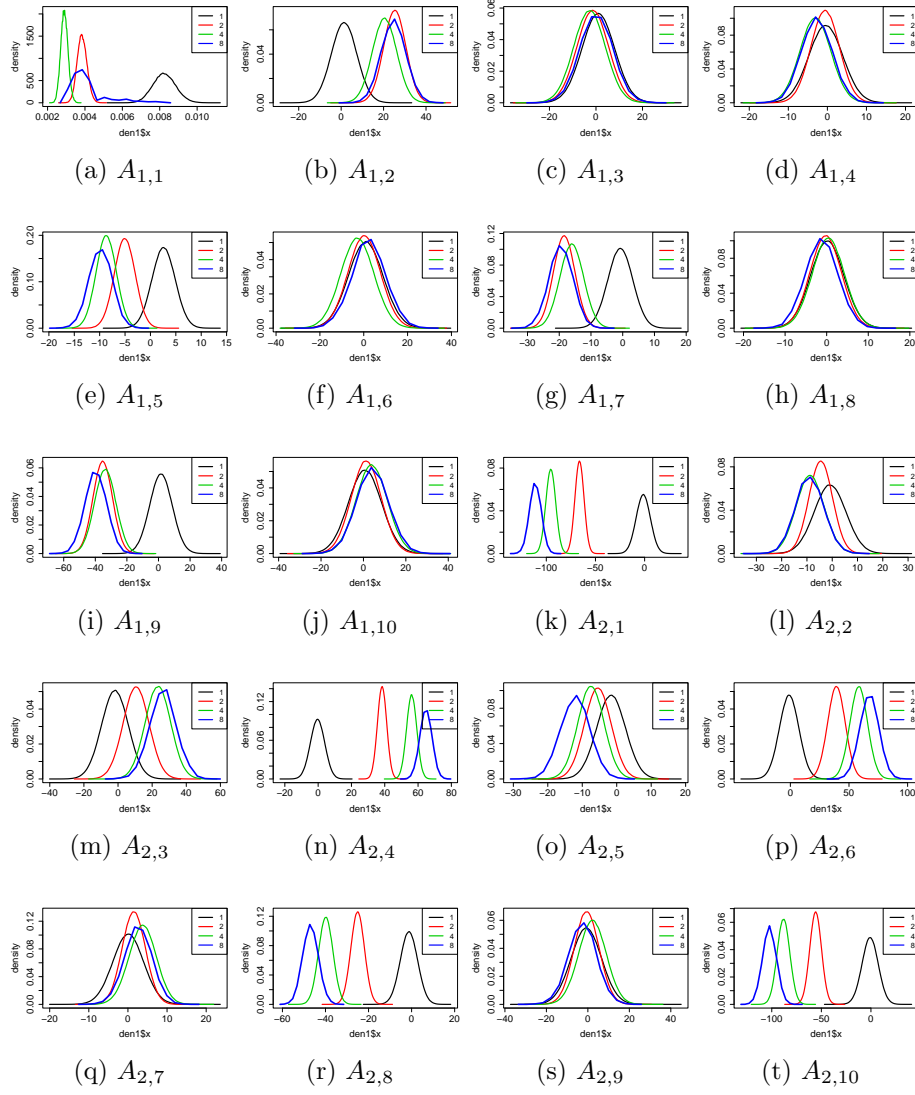


Figure 8: Posterior estimates of drift parameters for two dimensional cubic model fitted to the triad-Burgers equation for $\epsilon = 0.8$.

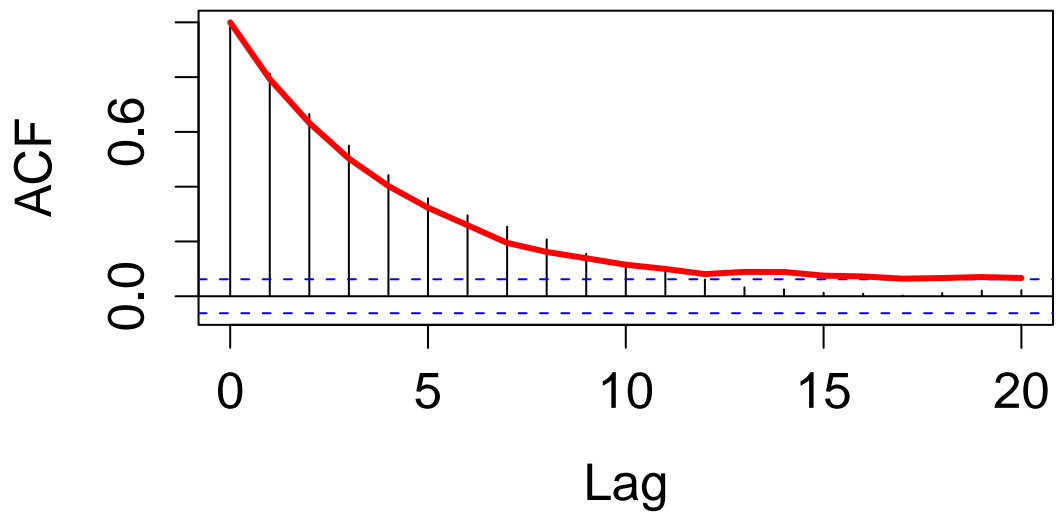


Figure 9: Autocorrelation plots of the full (vertical bars) and reduced (red) models for $\epsilon = 0.8$.

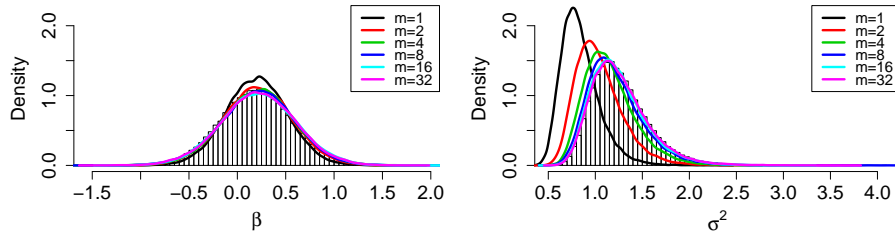


Figure 10: Posterior distributions for parameters from the OU process test data output from the GPU implementation (solid lines) compared with the exact posterior distributions (histograms).

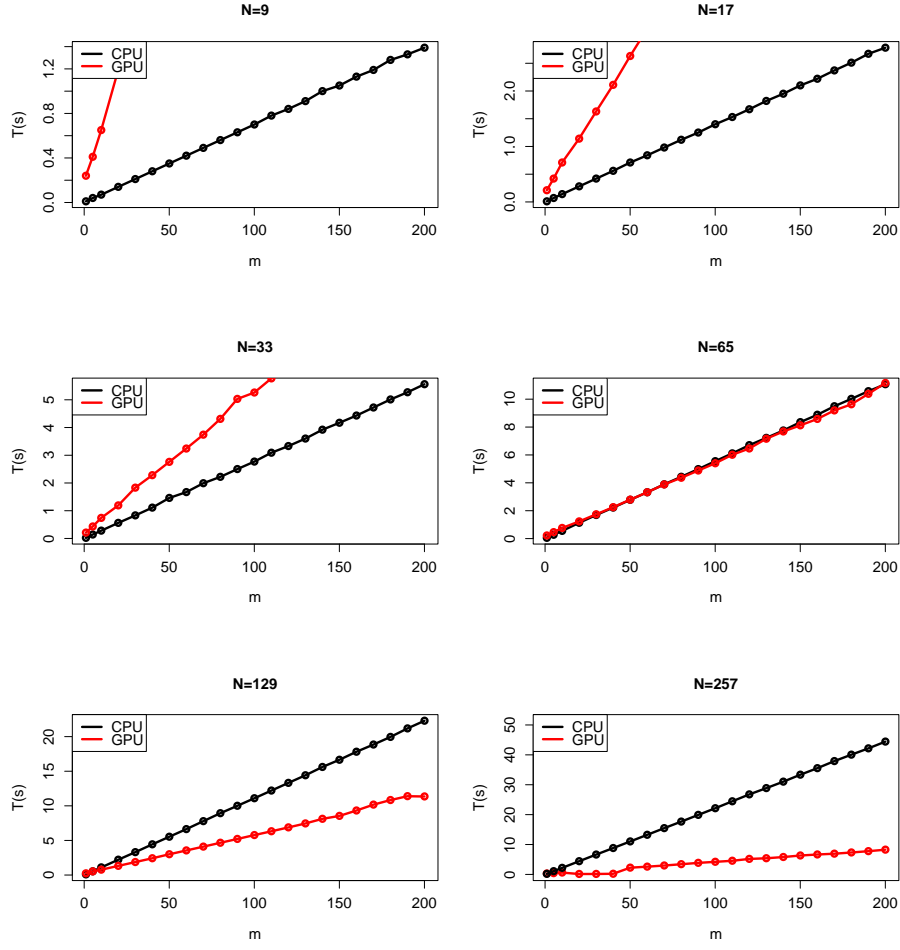


Figure 11: Real computation times to draw 1000 MCMC samples from the posterior distribution of the OU process for various size data sets. The time in seconds is plotted versus the amount of missing data for an implementation of the algorithm on a CPU and GPU.